Catal Surv Asia (2016) 20:167–172
DOI 10.1007/s10563-016-9217-7

Preparation and Photocatalytic Activity of SnO_2@TiO_2 Core–Shell Composites Modified by Ag

Jianguo Sheng[1] · Hebing Tong[1] · Hui Xu[1] · Cong Tang[1]

Published online: 8 July 2016
© The Author(s) 2016. This article is published with open access at Springerlink.com

Abstract Photocatalytic degradation is an important method to mediate organic pollution in the environment. This article reports Ag-modified SnO_2@TiO_2 core–shell composite photocatalysts prepared via a hydrothermal method. The Ag modification and core structure in the composite enhanced the photocatalytic activity and stability of TiO_2 in Rhodamine B degradation under visible light irradiation. The composite modified in 0.15 M $AgNO_3$ showed an optimal level of photocatalytic activity, as it degraded 99.14 % Rhodamine B in 60 min while pure TiO_2 only degraded 45.7 % during the same time.

Keywords Core–shell composites · Hydrothermal method · Photocatalytic activity

1 Introduction

Recently, titanium dioxide (TiO_2) has attracted great interest in the degradation of pollutants [1–3], such as most organic compounds and inorganic ions [4, 5]. However, the photocatalytic performance of TiO_2 is greatly restricted by its wide band gap (3.2 eV) and high electron–hole recombination rate. Proposed solutions to these problems include doping with metallic or nonmetallic ions [6, 7], dye photosensitization on the TiO_2 surface [8], deposition of noble metals [9, 10], and semiconductor modification [11].

Modifying TiO_2 with semiconductors such as SnO_2 has proven to be an effective way to improve the photocatalytic activity, by using the transport and separation of photoproduction carriers between two kinds of semiconductors with different energy gaps. Separately, Ag or other noble metals deposited on the surface of TiO_2 form a short-circuit battery with TiO_2, which leads to the effective separation of the photogenerated electrons/holes and lower potential in the reduction reaction, thus greatly improving the photocatalytic activity.

In this paper, Ag-modified SnO_2@TiO_2 core–shell composites were fabricated in two steps: first the synthesis of SnO_2@TiO_2 composite using a hydrothermal method, and then surface modification of the composite with Ag. The as-prepared samples demonstrated excellent photocatalytic activity and cycle stability under visible light.

2 Experimental

2.1 Preparation of Ag Modified SnO_2@TiO_2 Core–Shell Composites

2.1.1 Preparation of SnO_2

$SnCl_4{\cdot}5H_2O$ and polyethylene glycol (PEG) were added into deionized water and magnetically stirred. After $SnCl_4{\cdot}5H_2O$ was completely dissolved, excessive ammonia was added dropwise into the solution and stirred well. After filtration, washing, and calcination, the SnO_2 powder was obtained.

✉ Jianguo Sheng
sjg6418@sina.com

Hebing Tong
491490082@qq.com

Hui Xu
1069404605@qq.com

Cong Tang
1091334622@qq.com

[1] Institute of Environmental and Chemical Engineering, Jiangsu University of Science and Technology, Zhenjiang, Jiangsu, People's Republic of China

2.1.2 Preparation of SnO_2@TiO_2 core–shell composites

Tetrabutyl titanate, acetic acid, and anhydrous alcohol were mixed together, and then alcohol–water solution was slowly added to the mixture and stirred for 30 min. SnO_2 was then added, followed by another 30 min of stirring. The obtained solution was transferred to a 100 mL Teflon-lined autoclave and kept in an oven at 150 °C for 4 h. After cooling to room temperature, the precipitation was collected by centrifugation, washed with anhydrous alcohol, dried at 60 °C overnight. The obtained SnO_2@TiO_2 sample is designated as ST.

2.1.3 Preparation of Ag-Modified SnO_2@TiO_2 Core–Shell Composites

The ST composite was added to $AgNO_3$ solutions of different concentrations and irradiated under a 500 W mercury lamp. The precipitates were collected by centrifugation and dried at 60 °C overnight to obtain Ag-modified SnO_2@TiO_2 core–shell composites. The samples are designated as AgST-M, where M is the molar concentration of $AgNO_3$ solution used. For comparison, pure TiO_2 and Ag modified TiO_2 were synthesized separately, and labeled as PT and AgT.

2.2 Characterization of the Samples

The chemical composition of the samples was analyzed by energy dispersive X-ray spectroscopy (EDX, INCA). Transmission electron microscopy (TEM, JEM-2100, JEOL) was used for morphology characterization. The crystalline structures of the samples were determined by X-ray diffraction (XRD-6000, Japan Shimadzu) using Cu Ka radiation ($\lambda = 0.154$ nm) at 40 kV, 250 mA under room temperature. An X-ray photoelectron spectrometer (XPS, Thermo ESCALAB 250, Waltham, MA) was used to analyze the elemental composition and valence states. UV–vis diffuse reflectance spectra (DRS) of the samples was recorded in the range of 200–800 nm using a Shimadzu UV240 spectrophotometer (Kyoto, Japan) equipped with an integrating sphere, and $BaSO_4$ was used as the reference. Thermogravimetry and differential thermal analysis (TG–DTA) were performed by a Pyris Diamond 851e analyzer (PerkinElmer) at a heating rate of 20 °C min^{-1} under N_2 environment with a flow rate = 50 mL min^{-1}.

2.3 Photocatalytic Activity

The photocatalytic activities of the samples were evaluated by the degradation of Rhodamine B in a 500 mL jacketed beaker, and a 500 W mercury lamp was selected as the visible light source. In a typical experiment, 0.05 g of the as-prepared sample was dispersed in the Rhodamine B solution (40 mL, 5 mg L^{-1}). The solution was then maintained in the dark for 30 min prior to irradiation, in order to reach the adsorption–desorption balance. During irradiation, 4 mL of the sample solution was taken out every 10 min and analyzed by UV–vis spectroscopy. The degradation rate of Rhodamine B can be calculated via the formula: $\eta = (1 - A/A_0) \times 100\%$, where A_0 and A are the absorbance values of the original Rhodamine B solution and irradiated solution.

3 Results and Discussion

3.1 Phase Structure and Morphology Characterization

The XRD spectra of Ag-modified SnO_2@TiO_2 and comparison samples are shown in Fig. 1. Figure (ST) and (AgST) displayed the anatase phase of TiO_2 in $2\theta = 25.3°$, but it could not prove that the samples containing anatase phase of TiO_2, because there was only one peak. Mostly because of the low amount of TiO_2, X-ray diffraction (XRD) could not detect its presence. And no Ag peaks were detected in Figure (AgT) and (AgST), mostly due to the low amount of Ag [12–14].

Figure 2 shows the typical TEM images of AgST-0.15, showing that the as-prepared sample consists of many uniform and decentralized nanoparticles with diameters of 30–50 nm. The core–shell nanostructures can be observed in Fig. 2c, as the surface of SnO_2 nanoparticles is coated with a layer of TiO_2.

Figure 3a shows the TEM images of SnO_2 nanoparticles and Fig. 3b shows the TEM images of TiO_2 nanoparticles, it is showed the diameters of SnO_2 are 20–30 nm and the diameters of TiO_2 nano hybrids are about 400 nm, but these TiO_2 nano hybrids can disperse and cover SnO_2

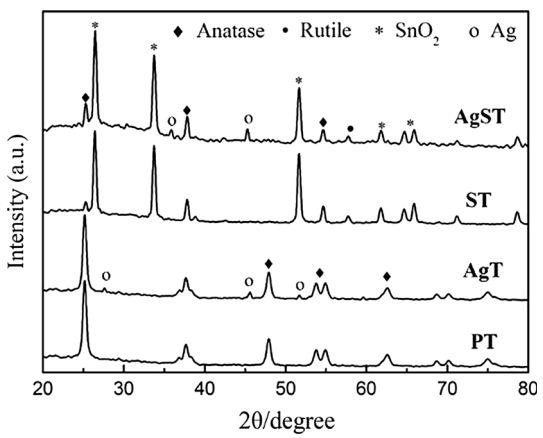

Fig. 1 XRD patterns of different samples

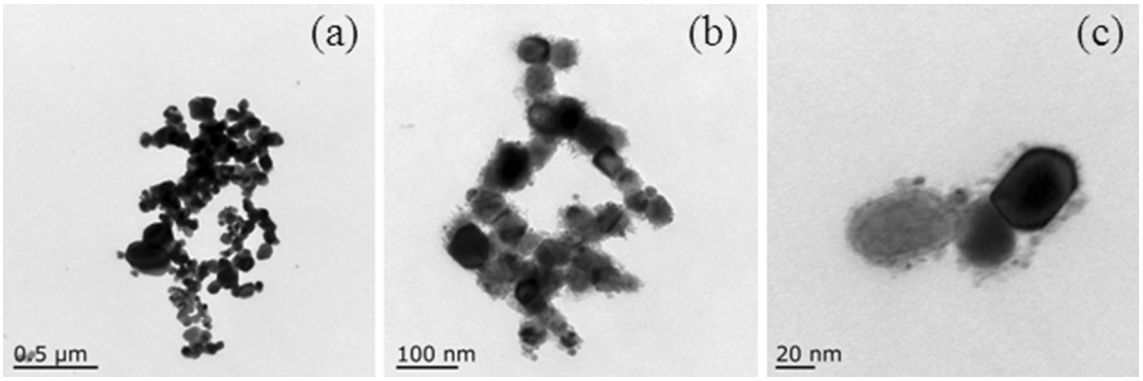

Fig. 2 TEM images of AgST-0.15 composite at different levels of magnification

nanoparticles. The diameters of Ag nanoparticles are also litter, so the diameters of AgST-0.15 are 30–50 nm.

3.2 Thermal Analysis-TG

TG–DTA curves of the Ag-modified SnO_2@TiO_2 core–shell nanoparticles are exhibited in Fig. 4. The results show that the nanoparticles undergo a multistep decomposition process in the temperature range of 25–800 °C. The endothermic peak in the temperature range of 25–90 °C is related to the desorption of physically adsorbed free water and residual ethanol, with about 8 % weight loss. The sharp exothermic peak in the temperature range of 200–300 °C is due to the combustion of organics on the surface of the sample. During this stage the weight loss percentage is about 5 %. In the temperature range of 300–400 °C there is another exothermic peak owing to further carbonization of organics and removal of constitution water. These results indicate that the as-prepared Ag-modified SnO_2@TiO_2 core–shell composite exhibits high thermal stability.

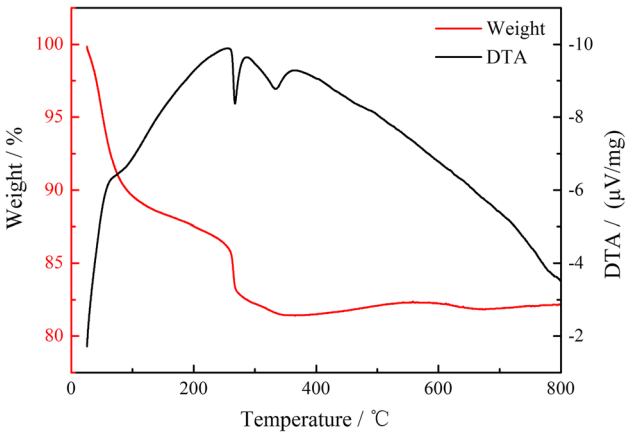

Fig. 4 TG-DTA *curves* of Ag-SnO_2@TiO_2 composite

3.3 Qualitative Elementary Analysis

AgST-0.15 was further analyzed by XPS to determine the main elements and their chemicals states on the TiO_2 surface. The survey spectrum is shown in Fig. 5a. The binding energies obtained in the analysis were corrected for

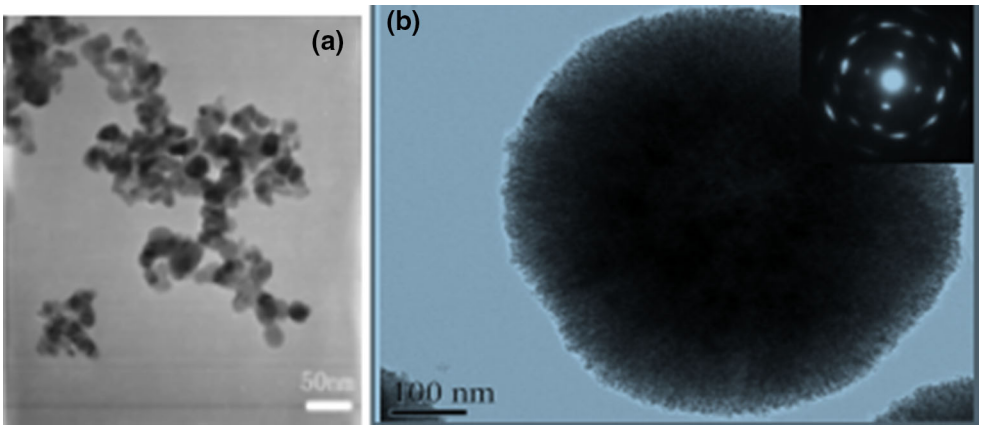

Fig. 3 TEM images of SnO_2 and TiO_2 nanoparticles

specimen charging by referencing C ls to 284.8 eV [15]. The results indicate the presence of five elements C, Ti, O, Sn, and Ag. Figure 5b shows the Sn 3d XPS spectrum. The two peaks centered at 495.2 and 486.9 eV correspond to the Sn $3d_{3/2}$ and Sn $3d_{5/2}$ peaks, respectively. The binding energy of Sn $3d_{5/2}$ (486.9 eV) matches the typical values for SnO_2 [16, 17], indicating that the Sn^{4+} dopant was incorporated into TiO_2 to form SnO_2. Figure 5c shows the XPS spectrum of Ag 3d. The binding energies of 368.2 and 374.2 eV were, respectively attributed to Ag $3d_{5/2}$ and Ag $3d_{3/2}$. The 6.0 eV slitting of the 3d doublet of Ag indicates the formation of metallic Ag on the surface of TiO_2 [18, 19]. The Ag content of AgST-0.3 estimated from XPS was 3.76 %. The atomic ratio of O/Ti determined from XPS is 2.82:1, which suggests the existence of oxygen vacancies on the surface of TiO_2.

The bandgap of composite SnO_2@TiO_2 became smaller compared with TiO_2 is because of the atomic orbital of Ti is $3d^2$,$4s^2$, and the atomic orbital of Sn is $5s^2$,$5p^2$, the four electrons of outer orbital of Ti will migrate to the outer orbital of Sn after they are all lost four electrons to form composite SnO_2@TiO_2, it can achieve the lowest energy for composite SnO_2@TiO_2. The deposition of Ag particles greatly increased the activity, the main reason is that the binding energies of Ag is lower than Sn and Ti(368.2 and 374.2 eV were, respectively attributed to Ag $3d_{5/2}$ and Ag $3d_{3/2}$), of course the activity depends on the loading amount of Ag, the energy is lower, the electronic migration is easier, the catalytic performance is better.

3.4 Photoelectrochemical Performances

3.4.1 UV–vis DRS Analysis

The activity of a photocatalyst mainly depends on the width of its band gap and the recombining rate of electron–hole pairs. From the UV–vis DRS results in Fig. 6, the band gaps for PT, AgT, ST, and AgST-0.3 are estimated to be 3.17, 3.06, 3.02, and 2.85 eV, respectively. Compared to PT, both AT and ST exhibited enhanced absorption extending towards the visible region. AgST-0.3 exhibited significant absorption of both ultraviolet and visible regions, revealing the synergistic effect of SnO_2 addition and Ag modification in narrowing the band gap of TiO_2. It can be ascribed to the following reasons: (1) the charge-transfer transitions between SnO_2 electrons and the TiO_2 conduction band [20, 21], (2) the incorporated metallic Ag serving as a delocalization energy level in the energy gap, which would extend the absorbance of TiO_2-based photocatalyst to the visible region [22].

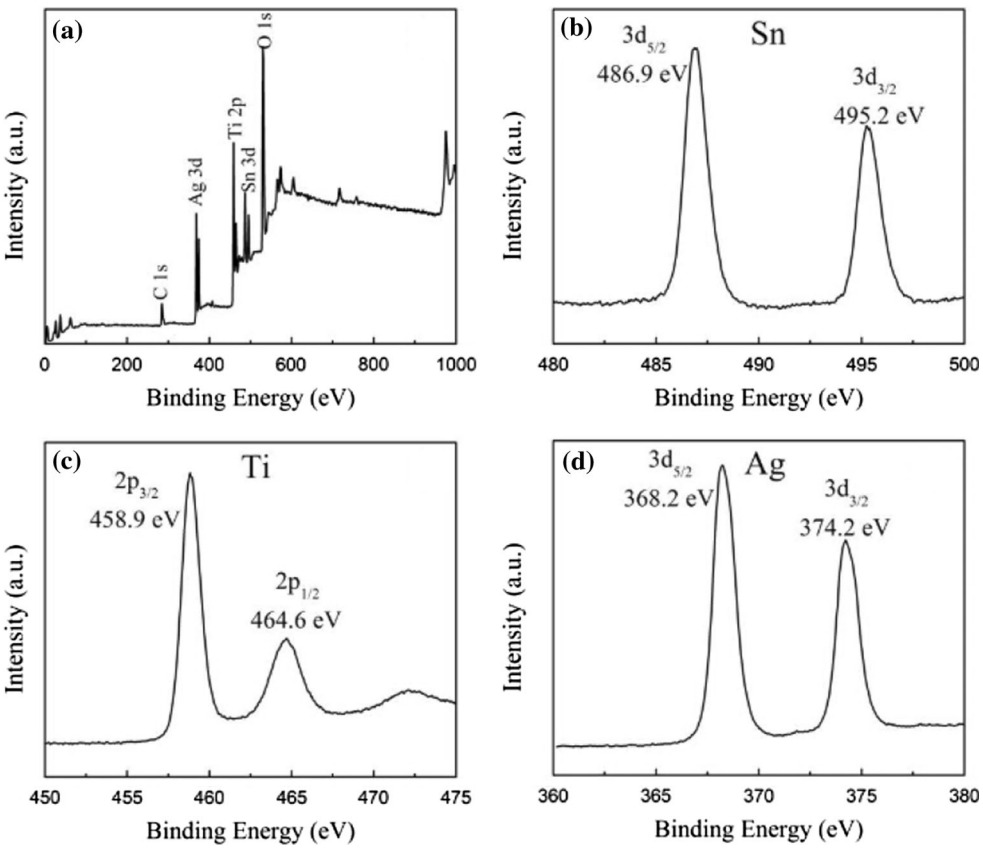

Fig. 5 XPS spectra of AgST-0.15: **a** survey spectra, **b** Sn 3d spectra, **c** Ti 2p spectra, **d** Ag 3d spectra

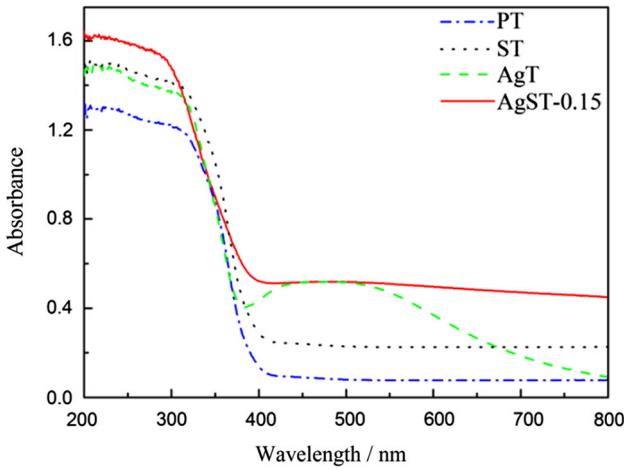

Fig. 6 UV–vis diffuse reflectance spectra of different samples

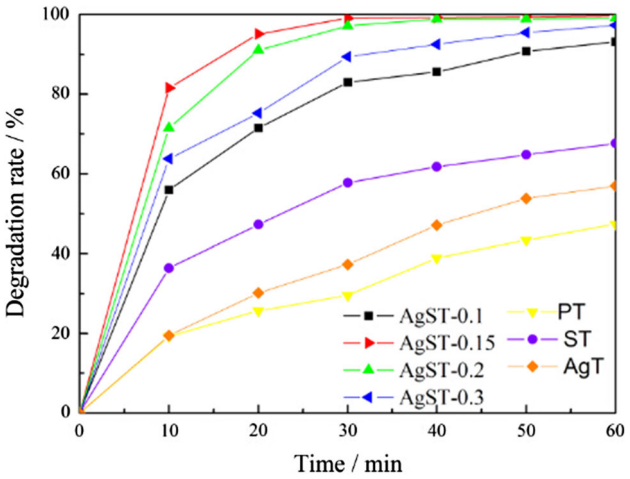

Fig. 7 The degradation curves of Rhodamine B under visible light irradiation with different photocatalysts

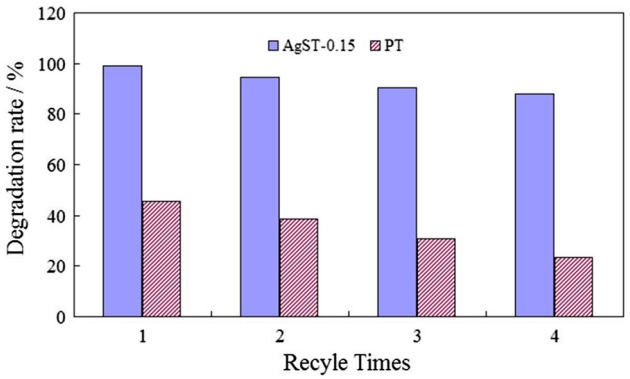

Fig. 8 Photochemical stability of AgST-0.15 and PT. The degradation rate is based on 60 min of reaction time

3.4.2 Photocatalytic Activity in Rhodamine B Degradation

The photocatalytic activities of the samples were evaluated by the degradation of Rhodamine B under visible light irradiation, and the results are shown in Fig. 7. Compared with PT, all modified TiO_2 samples show improved photocatalytic performance, especially the Ag-modified SnO_2@TiO_2 core–shell composites, which remarkably accelerated the photodegradation. Importantly, the photocatalytic efficiency initially increased with the concentration of $AgNO_3$ used for treatment, from 0 to 0.1 and then 0.15 M. Afterwards, the efficiency decreased with $AgNO_3$ concentration up to 0.3 M. The AgST-0.15 sample exhibited the best catalytic efficiency, which degraded 99.14 % of the Rhodamine B in 60 min, while PT degraded only 45.7 % during the same time.

3.5 Photochemical Stability of the Catalysts

Figure 8 compares the cycle stability of AgST-0.15 (the most effective Ag-modified catalyst) and unmodified PT. The activity of PT was approximately halved, from 45.7 to 23.63 %, after four catalytic cycles of 60 min each. In contrast, AgST-0.15 maintained a high level of catalytic activity after the same number of cycles.

4 Conclusion

Ag-modified SnO_2@TiO_2 core–shell composites were successfully prepared by a hydrothermal method. Compared with pure TiO_2, the composite sample had significantly improved photocatalytic activity in visible light, due to the synergistic effect of Ag modification and SnO_2 addition. Surprisingly, there is an optimal Ag content for improving the photocatalytic efficiency, beyond which the efficiency decreases. The sample modified with 0.15 M $AgNO_3$ possessed the best photocatalytic performance, as well as cycle stability.

Open Access This article is distributed under the terms of the Creative Commons Attribution 4.0 International License (http://creativecommons.org/licenses/by/4.0/), which permits unrestricted use, distribution, and reproduction in any medium, provided you give appropriate credit to the original author(s) and the source, provide a link to the Creative Commons license, and indicate if changes were made.

References

1. Fujishima A, Rao TN, Tyrk DA (2000) Titanium dioxide photocatalysis. J. Photochem Photobiol C Photochem Rev 1:1–21
2. Carp O, Huisman CL, Reller A (2004) Photoinduced reactivity of titanium dioxide. Prog Solid State Chem 32:33–177

3. Zhao J, Yang XD (2003) Photocatalytic oxidation for indoor air purification. Build Environ 38:645–654
4. Ohko Y, Saitoh S, Tatsuma T, Fujishima A (2001) Photoelectrochemical anticorrosion and self-cleaning effects of a TiO_2 coating for type 304 stainless steel. J Electrochem Soc 148:B24–B28
5. Subasri R, Shinohara T (2004) Application of the photoeffect in TiO_2 for cathodic protection of copper. Electrochemistry 72:880–884
6. Yuan JN, Tsujikawa S (1995) Characterization of sol-gel-derived TiO_2 coatings and their photoeffects on copper substrates. J Electrochem Soc 142:3444–3450
7. Song LZ, Zhao J, Wang XL (2005) Modification and anticorrosion property of carbon steel with TiO_2 film. J Iron Steel Res Int 12:37–41
8. Xie K, Sun L, Wang C, Lai Y, Wang M, Chen H, Lin C (2010) Photo electrocatalytic properties of Ag nanoparticles loaded TiO_2 nanotube arrays prepared by pulse current deposition. Electrochimica Acta 55:7211–7218
9. Li SN, Fu JJ (2013) Improvement in corrosion protection properties of TiO_2 coatings by chromium doping. Corros Sci 68:101–110
10. Lei CX, Liu Y, Zhou H, Feng ZD, Du RG (2013) Photogenerated cathodic protection of stainless steel by liquid-phase-deposited sodium polyacrylate/TiO_2 hybrid films. Corros Sci 68:214–222
11. Doslu ST, Mert BD, Yazici B (2013) Polyindole top coat on TiO_2 sol-gel films for corrosion protection of steel. Corros Sci 66:51–58
12. Lai YK, Zhuang HF, Xie KP, Gong DG, Tang YX, Sun L, Lin CJ, Chen Z (2010) Fabrication of uniform Ag/TiO_2 nanotube array structures with enhanced photoelectron-chemical performance. New J Chem 34:1335–1340
13. Liu Y, Hu J, Li J (2011) Synthesis and photoactivity of the highly efficient Ag species/TiO_2 nanoflakes photocatalysts. J Alloys Compd 509:5152–5158
14. Li X, Xiong R, Wei G (2009) Preparation and photocatalytic activity of nanoglued Sn-doped TiO_2. J Hazard Mater 164:587–591
15. Gao S, Li Z, Jiang K, Zeng H, Li L, Fang X, Jia X, Chen Y (2011) Biomolecule-assisted in situ route toward 3D superhydrophilic Ag/CuO micro/nanostructures with excellent artificial sunlight self-cleaning performance. J Mater Chem 21:7281–7288
16. Jia F, Sun W, Zhang J, Li Y, Yang B (2012) A facile approach to fabricate three-dimensional ordered macroporous rutile titania at low calcination temperature. J Mater Chem 22:2435–2441
17. Cao Y, Yang W, Zhang W, Liu G, Yue P (2004) Improved photocatalytic activity of Sn 4 + doped TiO_2 nanoparticulate films prepared by plasma-enhanced chemical vapor deposition. New J Chem 28:218–222
18. Liu Y, Wang X, Yang F, Yang X (2008) Excellent antimicrobial properties of mesoporous anatase TiO_2 and Ag/TiO_2 composite films. Microporous Mesoporous Mater 114:431–439
19. Wu M, Yang B, Lv Y, Fu Z, Xu J, Guo T, Zhao Y (2010) Efficient one-pot synthesis of Ag nanoparticles loaded on N-doped multiphase TiO_2 hollow nanorod arrays with enhanced photocatalytic activity. Appl Surf Sci 256:7125–7130
20. Zhao G, Cui X, Liu M, Li P, Zhang Y, Cao T, Li H, Lei Y, Liu L, Li D (2009) Electrochemical degradation of refractory pollutant using a novel microstructured TiO_2 nanotubes/Sb-doped SnO_2 electrode. Environ Sci Technol 43:1480–1486
21. Cao Y, Zhang X, Yang W, Du H, Bai Y, Li T, Yao J (2000) A bicomponent TiO_2/SnO_2 particulate film for photocatalysis. Chem Mater 12:3445–3448
22. Zhang F, Zheng Y, Zhan Y, Lin X, Zhang H, Zheng Q (2009) Studies on Ag-TiO2/KIT-6 composite nanosized photocatalyst. Spectrosc Spect Anal 29:2166–2170